

Adsorption Isotherms of Polyampholytes at Charged Spherical Particles<sup>†</sup>Ekaterina B. Zhulina, Andrey V. Dobrynin,<sup>‡</sup> and Michael Rubinstein\*

Department of Chemistry, University of North Carolina, Chapel Hill, North Carolina 27599-3290

Received: April 2, 2001; In Final Form: July 14, 2001

We develop a scaling theory of adsorption of polyampholyte chains at charged spherical particles from dilute low salt solutions. The adsorption is due to the polarization of polyampholyte chains in the electric field created by charged particles. The expressions for the surface coverage and the thickness of adsorbed layer are derived as functions of bulk polymer concentration, particle size, and surface charge density. We also describe the effect of the electric field of the particles on the dissociation equilibrium of adsorbed polyampholytes. The predictions of our scaling model are compared with the experiments on gelatin/latex systems.

## 1. Introduction

Polyampholytes are charged polymers carrying both positively and negatively charged monomers.<sup>1</sup> In solutions, these polymers may be anionic, cationic, or neutral (without net electric charge), depending on the solution pH. The advancements in understanding of these complicated polymeric systems have found applications in colloid stabilization, wetting, adhesion, and lubrication. In fact, the stabilizing properties of polyampholytes were recognized more than one hundred and fifty years ago by Faraday. He used gelatin, a polypeptide (protein) consisting of both basic and acidic amino acid groups, to stabilize gold colloidal particles.<sup>2</sup> This property of gelatin is successfully used by the photographic industry to stabilize silver halide sols<sup>3,4</sup> leading to extensive experimental<sup>5–12</sup> and theoretical<sup>13–16</sup> efforts toward understanding the unique features of polyampholyte adsorption at charged surfaces.

Recent theoretical studies<sup>14–16</sup> revealed a new mechanism of polyampholyte adsorption that is due to polarization of chains in the external electric field created by a charged object. The long-range polarization-induced attraction between polyampholyte chains and the charged object leads to multiple adsorbed polymer layers. The structure and thickness of these adsorbed layers depends on the charge distribution along the polyampholyte backbone, solution concentration, and such features of the particle surface as its curvature and surface charge density.

In our previous paper,<sup>17</sup> we reported the properties of the saturated adsorbed layers that are formed near charged planar and spherical surfaces in polyampholyte solutions close to their overlap concentration  $c^*$ . We demonstrated that the equilibrium structure of such layers is governed by the balance between the chain polarization in the electric field of the particle and the short-range nonelectrostatic interactions between monomers. We found that the adsorbed layers for large spherical particles are essentially the same as near planar charged surfaces.<sup>17</sup> However, the polarized molecules self-assemble into novel starlike structures near particles smaller than the Gaussian size of the

chains. The polyampholyte chains produce polarized loops that form “arms” of a “star” in the first adsorbed layer. The total number of such arms depends only on the fraction of charged monomers on polyampholyte backbone and the net charge of the particle but is independent of the chain molecular weight. The polymer density profile has a hyperbolic form similar to the distribution of monomers in a starlike polymer in a theta solvent.<sup>19,20</sup> At larger distances from the particle, the polarization of the chains decreases faster and the starlike structure of the adsorbed layer disappears.

In the present paper, we study the effect of the polyampholyte solution concentration on the structure of the adsorbed layer. In the framework of the scaling model, we derive the complete adsorption isotherm, i.e., the dependence of the adsorbed amount on the solution concentration for particles of different sizes and charges. In section 2, we describe our model. In section 3, we calculate the adsorption isotherm for particles of a given radius and surface charge density. We describe in detail the adsorption isotherms for two limiting cases of large (strongly charged) and small (weakly charged) particles. The isotherms corresponding to the intermediate values of particle sizes and charges are summarized in the Appendix. In section 4, we focus on the effect of the electric field of the particles on the ionization equilibrium of charged groups on the chain. Finally, in section 5, we discuss our results and compare them with experiments.

## 2. Model

**2.1. Polyampholyte Chain.** Consider a flexible polymer chain with the degree of polymerization  $N$ , bond length  $a$ , containing  $f_+N$  positive and  $f_-N$  negative elementary charges. The total number of charged groups per chain is  $f_+N + f_-N = fN$ . The chain can bear a small net charge  $e\Delta q = e(f_+N - f_-N)$ . The chain is immersed in a  $\theta$  solvent with zero second virial coefficient of nonelectrostatic monomer–monomer interactions and with the positive third virial coefficient of the order of  $a^6$ .

The attractive interactions between the charges of opposite sign could lead to a collapse<sup>21–24</sup> and precipitation of polyampholyte chains from solutions.<sup>25</sup> We focus here on the range of conditions for which polyampholyte molecules retain their Gaussian conformations with size  $R_0 \approx a\sqrt{N}$ . This is possible when the fluctuation-induced attractive interactions in the cloud

<sup>†</sup> Part of the special issue “Royce W. Murray Festschrift”.

\* To whom correspondence should be addressed.

<sup>‡</sup> Permanent address: Institute of Materials Science and Department of Physics, University of Connecticut, Storrs, CT 06269-3136.

of charged monomers are insufficient to cause the collapse of the chain. Assuming that the charges of both signs are distributed with average concentration  $c_{\text{ch}} \approx fN/R_0^3$  within the volume of a polymer coil, we find that the correlation-induced attraction energy  $W_{\text{att}} \approx -kT(l_B c_{\text{ch}})^{3/2} R_0^3$  does not perturb the Gaussian conformation of the polyampholyte chain when it is weaker than the thermal energy  $kT$

$$|W_{\text{att}}| \approx kT(fNl_B/R_0^3)^{3/2} R_0^3 \approx kTl_B^{3/2} a^{-3/2} f^{3/2} N^{3/4} < kT \quad (1)$$

Here,  $l_B = e^2/(\epsilon kT)$  is the Bjerrum length ( $e$  and  $\epsilon$  are the elementary charge and the dielectric constant of the solvent, respectively,  $k$  is the Boltzmann constant and  $T$  is the absolute temperature). The condition of weak fluctuation-induced attraction can be formulated as

$$f\sqrt{N}l_B/a \ll 1 \quad (2)$$

For example, for a polyampholyte chain with degree of polymerization  $N \approx 1000$  in a solution with the Bjerrum length  $l_B = 2a$ , the fraction of charged monomers should be  $f \leq a/(l_B\sqrt{N}) \approx 0.02$ . Below, we assume that inequality (2) is always satisfied.

**2.2. Electrostatic Potential near a Charged Sphere.** The charged spherical particle has radius  $R$  and the surface charge density  $e\sigma = eQ/(4\pi R^2)$ , where  $eQ$  is the total charge of the particle. We assume that the particle is positively charged  $Q > 0$ . The equal number of the monovalent counterions,  $Q$ , is distributed in solution around the particle. At small distances  $r - R \ll R$  from the surface of the sphere, its curvature is not important, and the dimensionless electrostatic potential can be approximated by that of a planar surface with the charge density  $e\sigma$ <sup>26,27</sup>

$$\Psi(r) = \frac{e\psi(r)}{kT} \approx \frac{l_B Q}{R} - 2 \ln\left(1 + \frac{r - R}{\lambda}\right) \quad (3)$$

where

$$\lambda = \frac{1}{2\pi\sigma l_B} \quad (4)$$

is the Gouy–Chapman length, that determines the decay of the counterion density,  $n(r)$ , near a charged surface. The counterion density profile near a charged planar surface is

$$n(r) \approx \frac{1}{2\pi l_B (\lambda + r - R)^2}, \quad \text{for } r - R \ll R \quad (5)$$

The curvature of the surface modifies the counterion distribution at distances  $r \geq 2R$  from the center of the particle. By calculating the number of counterions in the layer of thickness  $R$ , we can find the effective charge  $Q_{\text{eff}}$  at distance  $2R$  from the center of the sphere as

$$Q_{\text{eff}} \approx Q - 4\pi \int_R^{2R} n(r)r^2 dr \approx Q \frac{\lambda}{\lambda + R} \quad (6)$$

The relative values of the particle size  $R$  and the Gouy–Chapman length  $\lambda$  determine the effective charge  $Q_{\text{eff}}$  of the particle.

**Weakly Charged (Small) Particles ( $\lambda \gg R$ ).** The Gouy–Chapman length  $\lambda$  is larger than the particle size  $R$ , for weakly charged small spheres, and the effective charge  $Q_{\text{eff}}$  is of the order of the bare charge  $Q$  on the charged particle. The dimensionless electrostatic potential at distances  $r - R \ll R$

from the particle surface is obtained by expanding the right-hand side of eq 3 in the power series of  $(r - R)/\lambda$

$$\Psi(r) \approx \frac{l_B Q}{R} - 2 \frac{r - R}{\lambda} \approx \frac{l_B Q}{R} \ll 1, \text{ for } r - R \ll R \quad (7)$$

Thus, for large Gouy–Chapman lengths  $\lambda \approx (l_B \sigma)^{-1} \gg R$ , or for relatively small spherical particles, the presence of counterions near these particles can be neglected. This condition (eq 7) can be rewritten as  $Q \ll R/l_B$ . The Bjerrum length  $l_B$  in water at room temperature is 7 Å. Therefore, weakly charged particles of size  $R = 1$  nm may have at most one elementary charge, whereas weakly charged particles of size  $R = 10$  nm should have less than 15 elementary charges and surface charge density  $\sigma$  lower than  $\sigma \approx Q/(4\pi R^2) \approx 10^{-2} \text{ nm}^{-2}$ .

At large distances  $r \gg 2R$ , the electrostatic potential coincides with that for the unscreened charged sphere

$$\Psi(r) \approx \frac{l_B Q}{r} + C_1, \quad \text{for } R \ll r \quad (8)$$

where the constant  $C_1 = Ql_B/(2R) - 2R/\lambda$  ensures the continuity of the electrostatic potential at  $r \approx 2R$ .

**Strongly Charged (Large) Particles ( $\lambda \ll R$ ).** If the Gouy–Chapman length  $\lambda$  is much smaller than the size of the particle  $R$ , the counterions are localized inside the planar regime  $r - R \ll R$ . The effective charge on the sphere, felt by the rest of the solution, saturates at

$$Q_{\text{eff}} \approx R/l_B \quad (9)$$

and does not depend on the bare charge  $Q$  on the particle. For example, particles with size  $R \approx 68$  nm and surface charge density  $\sigma \approx 1.2 \text{ nm}^{-2}$  have bare charge  $Q \approx 7 \times 10^4$  and effective charge  $Q_{\text{eff}} \approx 100$  almost 3 orders of magnitude lower.

At distances  $r \gg 2R$ , the electrostatic potential is that of a charged sphere with the effective charge  $Q_{\text{eff}}$

$$\Psi(r) \approx \frac{l_B Q_{\text{eff}}}{r} + C_2 \approx \frac{R}{r} + C_2 \quad (10)$$

whereas at distances  $r - R \ll R$ , the potential is described by eq 7. As before, the constant  $C_2 \approx l_B Q/R - 2 \ln(1 + R/\lambda)$  ensures the continuity of the two expressions at  $r \approx 2R$ . Below, we use these potentials (eqs 3, 7, and 10) to calculate the polarization of polyampholyte chains near charged spherical particles.

### 3. Adsorption Isotherms

Equilibrium adsorption of polyampholyte molecules at charged particles implies the equality of the chemical potentials of polymer chains in the bulk solution  $\mu_B$ , and in the adsorbed layers  $\mu$ ,  $\mu_B = \mu$ . Far from the particles, polyampholyte molecules do not “feel” the electric field of the particles, and their chemical potential is determined by the translational entropy of chains in the dilute solution with polymer concentration  $c_B$

$$\mu_B = kT \ln(c_B/N) \quad (11)$$

The chemical potential of an adsorbed polyampholyte molecule with its center of mass located at distance  $x$  from the surface has the following form:

$$\frac{\mu(x)}{kT} = \ln\left(\frac{c(x)}{N}\right) + Na^6 c(x)^2 + \frac{W_{\text{pol}}^{\text{ch}}(x) + W_{\text{el}}^{\text{ch}}(x)}{kT} \quad (12)$$

where  $c(x)$  is the polymer concentration at distance  $x$  from the surface of the particle. The first term on the right-hand side of eq 12 accounts for the translational entropy of the chain within the adsorbed layer. The second term is due to nonelectrostatic interactions (ternary contacts) between monomers of adsorbed chains. The third term is the polarization energy of the polyampholyte in the electrostatic field of the particle, and the fourth one is the electrostatic interaction energy of the net charge  $e\Delta q$  of the polyampholyte chain with the particle. (For purely symmetric polyampholytes,  $\Delta q = 0$  and this term is equal to zero.) All of the numerical prefactors are omitted. In equilibrium,  $\mu_B = \mu$ , and the local polymer concentration,  $c(x)$ , is related to the solution concentration,  $c_B$

$$\ln\left(\frac{c(x)}{c^*}\right) + \left(\frac{c(x)}{c^*}\right)^2 \approx \ln\left(\frac{c_B}{c^*}\right) - \frac{W_{\text{pol}}^{\text{ch}}(x) + W_{\text{el}}^{\text{ch}}(x)}{kT} \quad (13)$$

where  $x = r - R$  is distance from the surface of the particle and  $c^*$  is the overlap concentration

$$c^* \approx NR_0^{-3} \approx a^{-3} N^{-1/2} \quad (14)$$

Equation 13 has two asymptotic solutions depending on whether the chains in the adsorbed layer overlap forming semidilute layer ( $c(x) \gg c^*$ ) or do not overlap ( $c(x) \ll c^*$ ).<sup>28</sup>

In the case of nonoverlapping chains ( $c(x) \ll c^*$ ), the nonelectrostatic interactions (the second term in the left-hand side of eq 13) in this dilute adsorbed layer are negligible in comparison with the chain translational entropy (the logarithmic term in the left-hand side of eq 13), and the polymer density profile is given by the Henry law

$$c(x) = c_B \exp\left[-\frac{W_{\text{pol}}^{\text{ch}}(x) + W_{\text{el}}^{\text{ch}}(x)}{kT}\right], \quad \text{for } H^* < x < H \quad (15)$$

where  $H$  is the layer thickness and  $H^*$  is the lower boundary of the dilute adsorbed layer.

The thickness of the adsorbed layer  $H$  is defined as the distance from the particle surface at which the polymer concentration  $c(H)$  is of the order of the solution concentration  $c_B$ . At this distance  $x \approx H$  from the particle surface, the sum of polarization  $W_{\text{pol}}^{\text{ch}}(H)$  and electrostatic  $W_{\text{el}}^{\text{ch}}(H)$  interaction energy of the chain is of the order of the thermal energy  $kT$ .<sup>16</sup> At length scales  $x \ll H$ , polyampholytes are strongly attracted by the adsorbing surface with the energy much larger than the thermal energy  $kT$ . Note that the adsorbed chains (strongly attracted to the surface) do not have to be in contact with the particle because of the long-range nature of polarization-induced attraction. It is interesting to point out that, for asymmetric polyampholytes with the net charge  $e\Delta q > 0$  (i.e., for molecules with the same sign of the net charge as the one on the particles,  $W_{\text{el}}^{\text{ch}}(x) > 0$ ), the adsorption can still occur at distances  $x$  where the absolute value of polarization energy  $|W_{\text{pol}}^{\text{ch}}(x)|$  of the chain is larger than the energy of electrostatic repulsion  $W_{\text{el}}^{\text{ch}}(x)$ . For oppositely charged polyampholytes ( $e\Delta q < 0$ ), the adsorption is enhanced by the direct electrostatic attraction between charged chains and the oppositely charged adsorbing particle.

The lower boundary  $H^*$  of the dilute adsorbed layer is defined as the length scale where the polymer concentration  $c(H^*)$  is of the order of the overlap concentration  $c^*$ . The thickness  $H^*$  of the semidilute part of the adsorbed layer is controlled by the

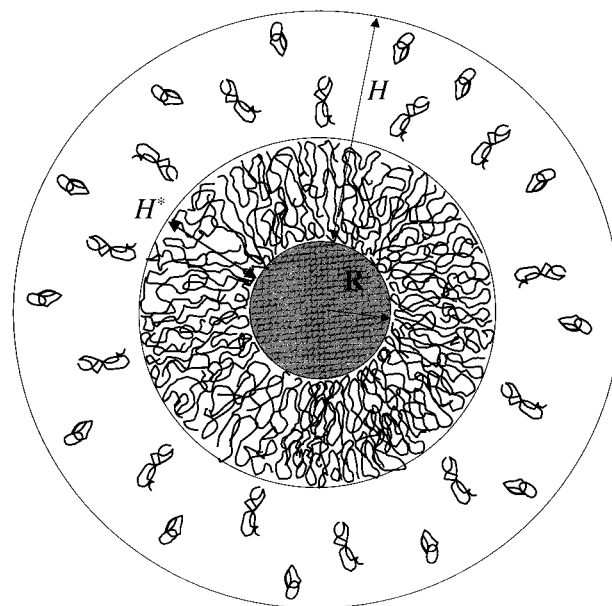


**Figure 1.** Schematic sketch of the structure of the adsorbed layer at a charged spherical particle.

solution concentration  $c_B$  and is a solution of eq 15 with  $c(H^*) \approx c^*$

$$W_{\text{pol}}^{\text{ch}}(H^*) + W_{\text{el}}^{\text{ch}}(H^*) \approx kT \ln(c_B/c^*) \quad (16)$$

The semidilute part of the adsorbed layer disappears at all ( $H^* \approx 0$ ) if the solution concentration  $c_B$  is lower than the crossover concentration  $c_B^{H^*}$  defined as

$$c_B^{H^*} \approx c^* \exp\left[\frac{W_{\text{pol}}^{\text{ch}}(0) + W_{\text{el}}^{\text{ch}}(0)}{kT}\right] \quad (17)$$

This crossover concentration  $c_B^{H^*}$  is the upper boundary of the Henry regime. In the Henry regime at solution concentrations  $c_B < c_B^{H^*}$ , there is no “semidilute” part of the adsorbed layer. At solution concentrations  $c_B > c_B^{H^*}$  on length scales  $x < H^*$ , the chains are crowded near the particle forming a semidilute part of the adsorbed layer ( $c(x) > c^*$ ). In this layer the nonelectrostatic (e.g., three-body) interactions are important. The polymer density profile in the inner semidilute part of the adsorbed layer is determined by the balance of the nonelectrostatic interactions between monomers (second term in the left-hand side of eq 13) and the polarization of a chain in the external electric field of the charged particles. Neglecting the first term in the left-hand side of eq 13 in comparison with the second term, one can write the concentration profile in the semidilute part of adsorbed layer

$$c(x) \approx c^* \sqrt{\ln\left(\frac{c_B}{c^*}\right) - \frac{W_{\text{pol}}^{\text{ch}}(x) + W_{\text{el}}^{\text{ch}}(x)}{kT}}, \quad \text{for } x < H^* \quad (18)$$

The logarithmic term in the right-hand side of the eq 18 is important only near the crossover to the dilute regime at  $x \approx H^*$  and can be safely omitted at the length scales  $x \ll H^*$  deep in the semidilute region.

At solution concentrations  $c > c_B^{H^*}$ , the majority of monomers are in the inner semidilute part of the layer of thickness  $H^*$  (see Figure 1) and most of the properties of adsorbed layer are determined by this part. Therefore, experimentally measured layer thickness is typically of the order of  $H^*$  rather than the

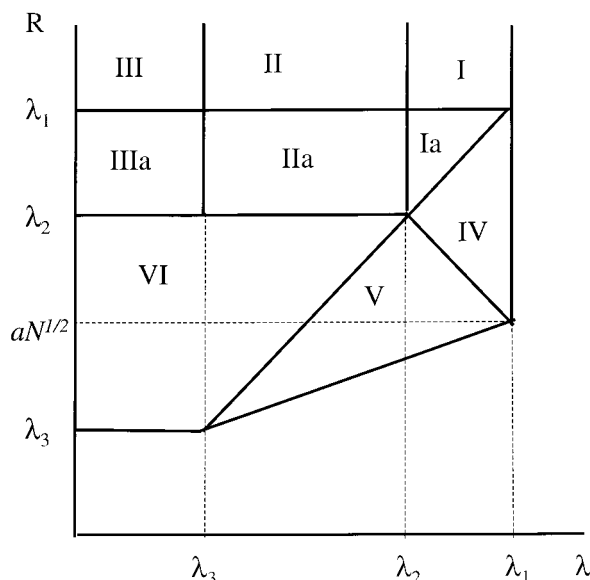


**Figure 2.** Adsorption diagram of polyampholyte chains as a function of the Gouy–Chapman length  $\lambda$  and the particle size  $R$ . Logarithmic scales. **Region I:** Stretched Planar Multilayers. **Region II:** Planar Pseudobrush + Stretched Multilayers. **Region III:** Planar Saturated Pseudobrush + Stretched Multilayers. **Regions Ia, IIa, and IIIa:** Spherical Multilayers + Adsorbed Layers of Regimes I, II, and III; **Region IV:** Weakly Charged Particles, Spherical Multilayers; **Region V:** Weakly Charged Particles, Pseudostar + Spherical Multilayers; **Region VI:** Strongly Charged Particles, Pseudostar + Spherical Multilayers.

thermodynamic layer thickness  $H$ . However, the dilute part of the adsorbed layer for  $H^* < x < H$  still exists, even though it does not influence most of its properties. In the Henry regime ( $c_B < c_B^{H^*}$ ), the experimentally measured thickness of the adsorbed layer depends on the experimental technique used to measure it.

The excess adsorbed amount per unit area,  $\Gamma$ , can be obtained by integration of the polymer density profile over the thickness of the adsorbed layer  $H$ :

$$\Gamma \approx \int_0^H [c(x) - c_B](1 + x/R)^2 dx \quad (19)$$

If the semidilute part of the adsorbed layer is present ( $c_B > c_B^{H^*}$ ), it determines the polymer adsorbed amount, whereas the contribution from the dilute part of the layer is very small.

**3.1. Adsorption Diagram.** The results of our previous studies<sup>17,18</sup> indicate that the polarization energy of the chain  $W_{\text{pol}}^{\text{ch}}(x)$  depends on the size and the charge density of the particle and the distance  $x$  from its surface. Below we summarize the results of ref 17 that are used in the derivation of the adsorption isotherms. Figure 2 reproduces the adsorption diagram from ref 17 which is plotted in the particle size  $R$ , Gouy–Chapman length  $\lambda \approx R^2/l_B Q$  coordinates.

**Region I (Stretched Planar Multilayers.**  $\lambda_2 < \lambda < \lambda_1$ ,  $\lambda_1 < R$ ). (The parameters  $\lambda_1$  and  $\lambda_2$  are defined by eqs 22 and 26 below.) Polyampholyte chains in this region are polarized and stretched by the external electric field of the particle. The size  $L(x)$  of the polyampholyte chain at distance  $x$  from the surface of the particle can be estimated by balancing the elastic stretching energy  $kTL(x)^2/a^2N$  with the electrostatic energy of the dipole of two opposite charges  $\pm e\sqrt{fN}$  of the two halves of the chain separated by the distance  $L(x)$  in the external electric field  $eE(x)/kT = -d\Psi(x)/dx$ , where the electrostatic potential  $\Psi(x)$  is given by eq 3:<sup>14,15</sup>

$$E(x)e\sqrt{fN}L(x) \approx kT \frac{\sqrt{fN}L(x)}{\lambda + x} \approx kT \frac{L(x)^2}{a^2N} \quad (20)$$

For this type of polyampholytes, the balance leads to the size of the chain perpendicular to the surface of the adsorbing particle

$$L(x) \approx \frac{R_0^2 \sqrt{fN}}{\lambda + x} \approx R_0 \frac{\lambda_1}{\lambda + x} \quad (21)$$

where we have introduced the threshold Gouy–Chapman length

$$\lambda_1 \approx R_0 \sqrt{fN} \quad (22)$$

The polarization energy of the chain is

$$W_{\text{pol}}^{\text{ch}}(x) \approx -kT \frac{L(x)^2}{a^2N} \approx -kT \left( \frac{\lambda_1}{x + \lambda} \right)^2 \quad (23)$$

This polarization energy is of the order of the thermal energy  $kT$  at length scales of the order of  $\lambda_1$ . The threshold Gouy–Chapman length  $\lambda_1$  defines the adsorption boundary. The adsorbed polyampholytes form a multilayer of stretched chains of thickness

$$H \approx \lambda_1 \quad (24)$$

(see Figure 3).

**Region II (Planar Pseudobrush + Stretched Multilayers.**  $\lambda_3 < \lambda < \lambda_2$ ,  $\lambda_1 < R$ ). (The parameter  $\lambda_3$  is defined by eq 28 below). Close to the surface at distances  $x < \lambda$ , the electric field created by the charged particle is almost constant. The sections of the chains are uniformly stretched up to length scales of the order of the Gouy–Chapman length  $\lambda$ . On length scales  $\lambda < x < \lambda_2$ , the polyampholytes are stretched into a self-similar pseudobrush (see Figure 4). The stretching of a subsection containing  $g(x)$  monomers with size  $x_g$  can be estimated by balancing the elastic energy of this subsection  $kTx^2/(a^2g(x))$  by its polarization energy  $e\sqrt{fg(x)x}E(x)$ . At length scales  $x > \lambda$ , the electric field  $E(x) \approx e/(\epsilon l_B x)$  is inversely proportional to the distance  $x$  from the surface. The relation between the strand size  $x$  and the number of monomers  $g(x)$  in it is given by the following equation:

$$x_g \approx a\sqrt{g(fg)}^{1/4}, \quad \text{for } \lambda < x_g < \lambda_2 \quad (25)$$

The size of the polymer chains in the first adsorbed layer is of the order of

$$\lambda_2 \approx x_N \approx R_0(fN)^{1/4} \quad (26)$$

It is important to point out that there are no loops with sizes smaller than the Gouy–Chapman length  $\lambda$ .<sup>17</sup> This is due to the fact that a loop with  $g_\lambda = \lambda^{4/3}a^{-4/3}f^{-1/3}$  monomers will have the lowest free energy in the constant electric field  $E \approx e/(\epsilon l_B \lambda)$  inside the Gouy–Chapman length  $\lambda$ . In fact, the probability to find a smaller loop is exponentially low.<sup>17</sup>

The polarization energy per strand of  $g$  monomers is proportional to  $-kT\sqrt{fg(x)}$ . The polarization energy  $W_{\text{pol}}^{\text{ch}}(x)$  of a polyampholyte chain of  $N/g(x)$  loops with the center of mass located at distance  $x$  from the surface is equal to

$$\frac{W_{\text{pol}}^{\text{ch}}(x)}{kT} \approx -\frac{N}{g(x)}\sqrt{fg(x)} \approx -N\sqrt{\frac{f}{g(x)}} \approx -N\left(\frac{af}{x + \lambda}\right)^{2/3}, \quad \text{for } 0 < x < \lambda_2 \quad (27)$$



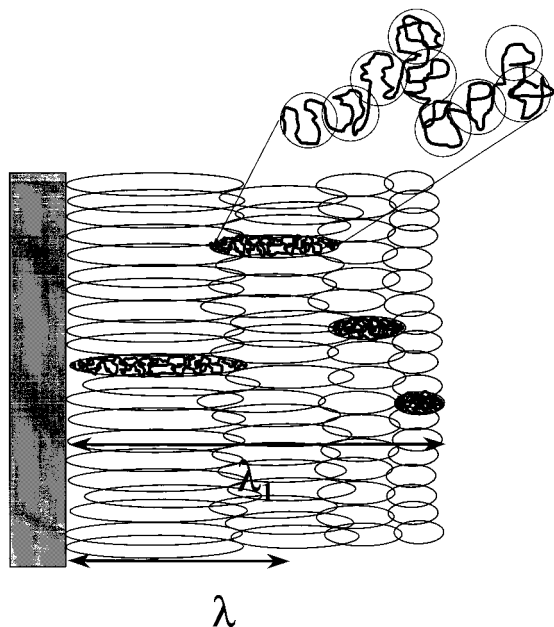


Figure 3. Schematic sketch of multilayer of stretched chains.

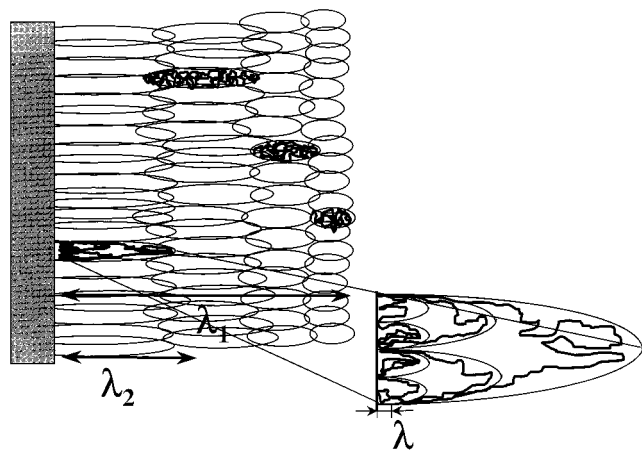


Figure 4. Schematic sketch of the configurations of polyampholyte chains in the adsorbed layer. The self-similar stretched pseudobrush at distances from the surface  $x < \lambda_2$  and the multilayer of stretched chains at  $\lambda_2 < x < \lambda_1$ .

Adsorbed polyampholyte chains form stretched planar multilayers at length scales larger than  $\lambda_2$ , similar to those in *region I* (see Figure 4), with the polarization energy of a chain  $W_{\text{pol}}^{\text{ch}}(x)$  given by eq 23. The crossover to *region III* takes place when the Gouy–Chapman length  $\lambda$  becomes of the order of the root-mean-square distance  $af^{-1/2}$  between charged monomers

$$\lambda_3 \approx af^{-1/2} \quad (28)$$

*Region III (Planar Saturated Pseudobrush + Stretched Multilayers.  $\lambda < \lambda_3, \lambda_1 < R$ ).* In this region, the Gouy–Chapman length  $\lambda$  is smaller than the root-mean-square distance  $af^{-1/2}$  between charged monomers along the chain. In this region, the monomers with the sign of the charge opposite to that of the surface are within distance  $\lambda$  from the surface, whereas the monomers with the charge of the same sign as the one of the surface are in the dangling loops. The average size of these loops can be estimated by comparing the repulsive force  $kT/x$  between the charges located at the distance  $x$  from the surface and the surface with the elastic force due to the stretching of the parts of the chain with  $f^{-1}$  monomers  $kTxf/a^2$ . At equilibrium,

these two forces are equal. This leads to the condition of almost unperturbed strands of size  $x \approx af^{-1/2}$ . Thus, near the charged surface inside a layer of thickness  $\lambda_3$ , the strands of polyampholytes are almost unperturbed by the external electric field. The polarization energy of a chain with center of mass located at the distances  $x$  from the adsorbing surface of the order of  $\lambda_3$  is approximately  $kT$  per charge

$$\frac{W_{\text{pol}}^{\text{ch}}(x)}{kT} \approx -Nf, \quad \text{for } 0 < x < \lambda_3 \quad (29)$$

On length scales between  $\lambda_3$  and  $\lambda_2$ , adsorbed polyampholytes form a self-similar pseudobrush similar to the one in *region II*, and on length scales  $\lambda_2 < x < \lambda_1$ , the adsorbed chains form planar multilayers of stretched chains similar to those in *region I*.

The crossover into new regions occurs when the particle size  $R$  becomes of the order of the thickness  $\lambda_1$  of the planar adsorbed layer. The line  $R \approx \lambda_1$  defines the boundary between regions I, II, III, and Ia, IIa, and IIIa in the adsorption diagram (Figure 2).

*Regions Ia, IIa, and IIIa (Spherical Multilayers + Adsorbed Layers of Regions I, II, and III).* In these regions, the curvature starts to affect the structure of the adsorbed layer at length scales  $x > R$ . At these length scales, adsorbed polyampholytes are polarized in the hyperbolic electrostatic potential created by the charged sphere and form spherical multilayers of stretched chains. The polarization energy of a polyampholyte chain for the case of screened Coulomb potential for strongly charged particles with  $Q_{\text{eff}} \approx R/l_B$  (see, for details, ref 17) is

$$\frac{W_{\text{pol}}^{\text{ch}}(x)}{kT} \approx -\frac{l_B Q_{\text{eff}} \sqrt{fN}}{x^2} L(x) \quad (30)$$

Once again the balance of the polarization energy of the chain and its elastic energy gives the chain size at the distance  $x$  from the surface of the particle:

$$L(x) \approx \frac{a^2 l_B Q_{\text{eff}}^{4/2} N^{3/2}}{x^2} \approx \frac{l_B Q_{\text{eff}} R_0^2 \sqrt{fN}}{x^2} \approx \frac{l_B Q_{\text{eff}} \lambda_1}{x^2} \quad (31)$$

Substituting this equilibrium chain size  $L(x)$  back into the expression (eq 30), we obtain the polarization energy of a polyampholyte chain

$$\frac{W_{\text{pol}}^{\text{ch}}(x)}{kT} \approx -\frac{(l_B Q_{\text{eff}} \lambda_1)^2}{x^4} \approx -\left(\frac{r_1}{x}\right)^4, \quad \text{for } R < x < r_1 \quad (32)$$

where

$$r_1 \approx \sqrt{l_B Q_{\text{eff}} \lambda_1} \quad (33)$$

The adsorption stops at the distances of the order of  $r_1$  where the polarization energy of a polyampholyte chain becomes of the order of the thermal energy  $kT$ . Close to the surface of the adsorbing particle, at length scales  $0 < x < R$ , the structure of the adsorbed layer is similar to the one in *regions I, II, and III* respectively.

*Region IV (Weakly Charged Particles, Spherical Multilayers.  $(\sqrt{fN}R < \lambda < \lambda_1)$ ).* In this region, the Gouy–Chapman length  $\lambda$  is larger than the particle size  $R$  and polyampholyte chains are polarized and stretched by the unscreened electrostatic potential of the charged sphere carrying charge  $eQ$  ( $Q_{\text{eff}} \approx Q$ ). The adsorbed polyampholyte chains form spherical multilayers of

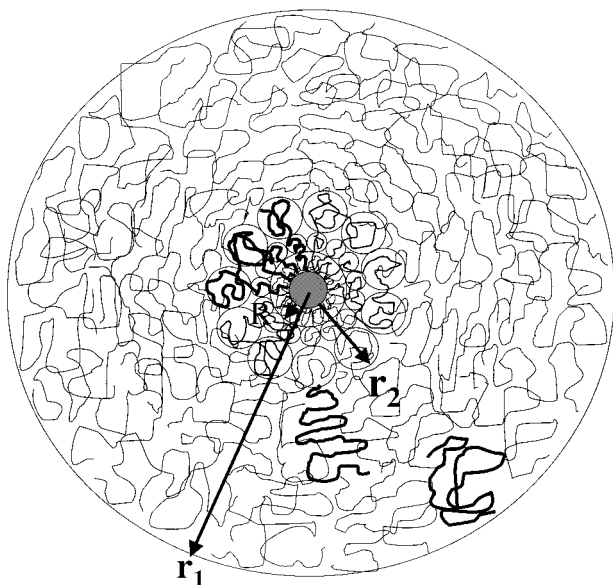


**Figure 5.** Schematic sketch of the structure of the adsorbed polyampholyte chains at a charged spherical particle.

stretched chains. The thickness of the adsorbed layer  $r_1$  increases with increasing charge  $Q$  of the particle.

**Region V (Weakly Charged Particles, Pseudostar + Spherical Multilayers.**  $R < \lambda < \sqrt{fNR}$ ,  $\lambda < \sqrt{fNR_0^2/R}$ ). Polyampholyte chains form a self-similar structure close to the particle surface similar to that of a neutral starlike macromolecule, with the number of arms  $n_{ch} \approx f^{2/3}(l_B Q/a)^{4/3}$  and with the degree of polymerization  $N$  each (see, for details, ref 17). This adsorbed state of polyampholytes is called a “pseudostar” (see Figure 5). The polarization energy of a loop containing  $g$  monomers with the center of mass located at distance  $x \gg R$  from the surface of the particle with the excess charges in two halves of the loop  $q \approx (fg)^{1/2}$  separated by the distance  $x$  is given by the following expression

$$\frac{W_{pol}^e(x)}{kT} \approx -\frac{l_B Q q}{x} \approx -\frac{\sqrt{fg(x)} l_B Q}{x} \quad (34)$$

The relation between the loop size  $x$  and the number of monomers  $g(x)$  in it is obtained by the balance of the loop polarization energy  $W_{pol}^e(x)$  (eq 34) with its elastic energy,  $W_{el} \approx kTx^2/ga^2$ , to give

$$x^2 \approx a^{4/3} f^{1/3} (l_B Q)^{2/3} g(x), \text{ for } R < x < r_2 \quad (35)$$

where the thickness of this first layer is equal to

$$r_2 \approx (a^2 l_B Q f^{1/2})^{1/3} N^{1/2} \quad (36)$$

The polarization energy  $W_{pol}^{ch}(x)$  of a chain in this pseudostar is equal to the average number of loops  $N/g(x)$  with  $g(x)$  monomers times the polarization energy of a loop  $W_{pol}(x) \approx -\sqrt{fg(x)} l_B Q/x$ :

$$\frac{W_{pol}^{ch}(x)}{kT} \approx -N \sqrt{\frac{f}{g(x)}} \frac{l_B Q}{x} \approx -N f^{2/3} \frac{(l_B Q)^{4/3} a^{2/3}}{x^2}, \text{ for } R < x < r_2 \quad (37)$$

It is important to point out that there are no loops with sizes smaller than the particle radius  $R$ .<sup>17</sup> This is due to the fact that a loop with  $g_R \approx R^2/(a^{4/3} f^{1/3} (l_B Q)^{2/3})$  monomers will have the

lowest free energy in the constant electric field  $E \approx eQ/(\epsilon R^2)$  at distances  $x < R$ . The expression for polarization energy of the chain that covers the whole range  $0 < x < r_2$  is

$$\frac{W_{pol}^{ch}(x)}{kT} \approx -N f^{2/3} \frac{(l_B Q)^{4/3} a^{2/3}}{(x+R)^2}, \text{ for } 0 < x < r_2 \quad (38)$$

On length scales  $r_2 < r < r_1$ , the adsorbed chains form spherical multilayer of stretched chains (see Figure 5) with the polarization energy of the chain  $W_{pol}^{ch}(x)$  given by eq 32.

**Region VI (Strongly Charged Particles, Pseudostar + Spherical Multilayers.**  $af^{-1/2} < R < \lambda_2$ ,  $\lambda < R$ ). In this region at length scales  $x$  between  $R$  and  $r_2$ , the adsorbed chains form a pseudostar. The corresponding equations for the size of this pseudostar  $r_2$  and chain polarization energy are obtained from eqs 36 and 38 by substituting particle charge  $Q$  in these equations by its effective value  $R/l_B$ . Close to the particle surface for  $0 < x < R$  the curvature of the adsorbing particle does not affect the structure of the adsorbed layer and polyampholytes form a planar pseudobrush.

As an example, consider a chain with  $N = 1000$  monomers, with the fraction of charges  $f = 0.02$ , and with the bond length  $a = 3 \text{ \AA}$  in the solution with the Bjerrum length  $l_B = 7 \text{ \AA}$ . The marginal Gouy–Chapman length for this polymer is  $\lambda_1 \approx 400 \text{ \AA}$ . The crossover to self-similar adsorbed layer occurs for it at  $\lambda_2 \approx 200 \text{ \AA}$ . Adsorbed layers are insensitive to the particle size for the particles with sizes  $R > 400 \text{ \AA}$  and have thickness  $\lambda_1 \approx 400 \text{ \AA}$ . However, for the particles with sizes  $R < 400 \text{ \AA}$ , the curvature of the particle becomes important. The thickness of the polymeric adsorbed layer around strongly charged particles with size  $R \approx 150 \text{ \AA}$  is  $r_1 \approx \sqrt{R\lambda_1} \approx 250 \text{ \AA}$ , and adsorbed chains form spherical adsorbed layers. Thus, varying particle size, one can access different regimes of the adsorption diagram.

**3.2. Adsorption Isotherms for Large Particles ( $R > \lambda_1$ ).** Consider large particles with radius  $R > \lambda_1$  in region II of the diagram in Figure 2.

**Henry Regime.** At extremely low solution concentrations of symmetric polyampholytes ( $\Delta q = 0$ ), the polymer density profile in the adsorbed layer is given by eq 15 with  $W_{el}^{ch}(x) = 0$  and  $W_{pol}^{ch}(x)$  given by eq 27 at length scales  $0 < x < \lambda_2$  and by eq 23 at  $\lambda_2 < x < \lambda_1$ . In this case, eq 15 for polymer density profile reduces to

$$c(x) \approx c_B \begin{cases} \exp\left[N\left(\frac{af}{x+\lambda}\right)^{2/3}\right], & \text{for } 0 < x < \lambda_2 \\ \exp\left[\left(\frac{\lambda_1}{x}\right)^2\right], & \text{for } \lambda_2 < x < \lambda_1 \end{cases} \text{ for } c_B < c_B^{H*} \quad (39)$$

where the upper boundary concentration  $c_B^{H*}$  of the Henry regime is defined by eq 41 below. The polymer concentration  $c(x)$  near the adsorbing surface becomes of the order of the solution concentration  $c_B$  at distances  $x \approx \lambda_1$ , where the polarization energy of a chain is of the order of the thermal energy  $kT$ . This defines the thickness of the adsorbed layer  $H \approx \lambda_1$ . Integrating the polymer density profile  $c(x)$  in the interval  $0 < x < \lambda_1$ , one finds the polymer surface coverage

$$\Gamma_{II} \approx \int_0^{\lambda_2} c_B \exp\left[N\left(\frac{af}{x+\lambda}\right)^{2/3}\right] dx + \int_{\lambda_2}^{\lambda_1} c_B \exp\left[\left(\frac{\lambda_1}{x}\right)^2\right] dx \quad (40)$$

$$\approx c_B \lambda \exp\left[N\left(\frac{af}{\lambda}\right)^{2/3}\right], \text{ for } c_B < c_B^{H*}$$

The surface coverage  $\Gamma_{II}$  is controlled by the layer of thickness  $H_{\text{char}}$  of the order of the Gouy–Chapman length  $\lambda$  and is proportional to the solution concentration  $c_B$ .

The crossover concentrations  $c_B^{H^*}$  between the Henry regime and pseudobrush regime of crowded chains is expected at solution concentration  $c_B \approx c_B^{H^*}$  at which the polymer concentration at the adsorbing surface  $c(0)$  reaches the overlap concentration  $c^*$ . Substituting  $c(0) \approx c^*$  into eq 39, we find the boundary of the Henry regime:

$$c_B^{H^*} \approx c^* \exp\left[-N\left(\frac{af}{\lambda}\right)^{2/3}\right], \quad \text{region II} \quad (41)$$

**Pseudobrush Regime.** Above solution concentration  $c_B^{H^*}$ , the nonelectrostatic interactions between monomers near the particle surface force chains to rearrange into the self-similar structures of polarized loops, called pseudobrushes. The thickness  $H^*$  of this semidilute inner adsorbed layer is obtained from eq 16 for  $W_{\text{el}}^{\text{ch}} = 0$  by substituting eq 27 for the chain polarization energy  $W_{\text{pol}}^{\text{ch}}(H^*)$

$$H^* \approx \frac{afN^{3/2}}{[\ln(c^*/c_B)]^{3/2}} - \lambda, \quad \text{for } c_B^{H^*} < c_B < c_B^{\lambda_2} \quad (42)$$

where the second threshold solution concentration  $c_B^{\lambda_2}$  is defined by eq 43 below. For solution concentrations  $c_B^{H^*} < c_B < c_B^{\lambda_2}$ , the thickness of the semidilute pseudo-brush part of the adsorbed layer  $H^*$  is less than its saturation value  $\lambda_2$ . The thickness  $H^*$  of this layer grows with solution concentration  $c_B$  and finally reaches the saturation value  $\lambda_2$  at concentration  $c_B^{\lambda_2}$

$$c_B^{\lambda_2} \approx c^* \exp(-\sqrt{fN}), \quad \text{region II} \quad (43)$$

The polymer density profile in this semidilute layer can be found by substituting eq 27 for the polarization energy in eq 18

$$c(x) \approx c^* \sqrt{\ln\left(\frac{c_B}{c^*}\right) + N\left(\frac{af}{x + \lambda}\right)^{2/3}}, \quad \text{for } 0 < x < H^* \quad (44)$$

However, at length scales  $x > H^*$ , there is still a dilute adsorbed layer with polymer density profile given by eq 39. Integrating the polymer density profile in the adsorbed layer, one finds the polymer surface coverage  $\Gamma_{II}$

$$\Gamma_{II} \approx \frac{fN}{a^2} \frac{1}{\ln(c^*/c_B)}, \quad \text{for } c_B^{H^*} < c_B < c_B^{\lambda_2} \quad (45)$$

The surface coverage is dominated by semidilute part of the adsorbed layer of thickness  $H^*$  and has a weak logarithmic dependence on solution concentration. At the upper boundary of the pseudobrush regime  $c_B \approx c_B^{\lambda_2}$ , the surface coverage is

$$\Gamma_{II}(c_B^{\lambda_2}) \approx \frac{\sqrt{fN}}{a^2} \quad (46)$$

**Multilayer Regime.** At higher, but still dilute solution concentrations  $c_B^{\lambda_2} < c_B < c^*$ , the thickness of the semidilute part of the adsorbed layer  $H^* > \lambda_2$  and this layer includes a multilayer of stretched chains in addition to a pseudobrush. There are three different parts in the adsorbed layer: pseudobrush at length scales  $0 < x < \lambda_2$  with polymer density given

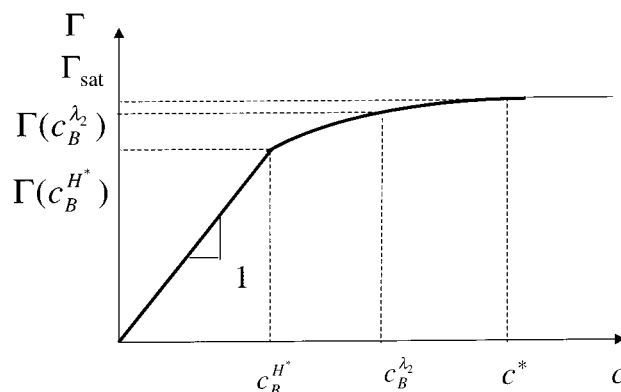


**Figure 6.** Dependence of the polymer surface coverage  $\Gamma$  on solution concentration for polyampholyte adsorption at large particles. Logarithmic scales.

by eq 44; semidilute multilayer at  $\lambda_2 < x < H^*$  with polymer density

$$c(x) \approx c^* \sqrt{\ln\left(\frac{c_B}{c^*}\right) + \left(\frac{\lambda_1}{x}\right)^2}, \quad \text{for } \lambda_2 < x < H^* \quad (47)$$

that is obtained by substituting the polarization energy per chain eq 23 into eq 18; dilute part at  $H^* < x < \lambda_1$  with polymer density given by eq 39. In multilayer adsorption regime, the thickness of the semidilute part of the adsorbed layer  $H^*$  is

$$H^* \approx \frac{\lambda_1}{\sqrt{\ln(c^*/c_B)}} \approx \frac{af^{1/2}N}{\sqrt{\ln(c^*/c_B)}} \quad (48)$$

Integration of the polymer density profile results in the following expression for the polymer surface coverage

$$\Gamma_{II} \approx \frac{\sqrt{fN}}{a^2} \ln\left[\frac{\lambda_1}{\lambda_2} \frac{1}{\sqrt{\ln(c^*/c_B)}}\right], \quad \text{for } c_B^{\lambda_2} < c_B < c^* \quad (49)$$

This weak double-logarithmic dependence of surface coverage on solution concentration  $c_B$  continues until  $c_B \approx c^*$  where the surface coverage reaches its saturation value

$$\Gamma_{II}^{\text{sat}} \approx \frac{\sqrt{fN}}{a^2} \ln(fN) \quad (50)$$

At saturation, the whole adsorbed layer is semidilute

$$H^* \approx H_{II}^{\text{sat}} \approx \lambda_1 \quad (51)$$

To summarize, for large particles with radius  $R > \lambda_1$ , the thickness of the adsorbed layer  $H$  does not depend on the surface charge density  $\sigma$  and the radius of the particles  $R$ . For dilute polyampholyte solutions  $c_B \leq c^*$ , the thickness  $H^*$  of the semidilute part of the adsorbed layer depends on the degree of polymerization  $N$ , the fraction of charged monomers on the chain  $f$ , and the solution concentration  $c_B$  (eqs 42 and 48). In the Henry regime, the polymer surface coverage is proportional to the bulk polymer concentration,  $\Gamma \sim c_B$  (see Figure 6), whereas in the “plateau” regimes (when  $c_B^{H^*} \leq c_B \leq c^*$ ),  $\Gamma(c_B)$  demonstrates weak logarithmic and double-logarithmic dependences on polymer concentration  $c_B$  (see Figure 6).

**Asymmetric Polyampholytes.** Consider the effect of charge asymmetry  $\Delta q > 0$  on the polyampholyte adsorption. The presence of the net charge  $\Delta q > 0$  on the polyampholyte chain with the same sign as the charge on adsorbing particles reduces

the adsorption due to direct electrostatic repulsion between polyampholyte chains and the particle ( $W_{\text{el}}^{\text{ch}}(x) > 0$ ). Near the surface of large charged particles with radius  $R > \lambda_1$ , the electrostatic potential is described by eq 3. Therefore, the energy of electrostatic repulsion between the particle and the net charge  $\Delta q$  on the chain with the center of mass located at distance  $x$  from the surface is given by

$$W_{\text{el}}^{\text{ch}}(x)/kT = \Delta q[\Psi(x) - \Psi(r_D)] \approx 2\Delta q \ln\left(\frac{\lambda + r_D}{\lambda + x}\right) \quad (52)$$

where  $r_D = 1/\sqrt{4\pi l_B \sum z_i^2 c_i}$  is the Debye screening length in the system with concentration  $c_i$  of ions of valency  $z_i$ . Even in the salt-free solutions (with no added salt) this screening length is finite and is governed by the concentration of polyampholytes and counterions. Below, we use eq 52 to determine the changes in the adsorbed layer due to the charge asymmetry.

For example, in the Henry regime, the polymer concentration in the adsorbed layer is

$$c(x) = c(x) \approx c_B \begin{cases} \exp\left[N\left(\frac{qf}{x+\lambda}\right)^{2/3} - 2\Delta q \ln\left(\frac{\lambda+r_D}{\lambda+x}\right)\right], & \text{for } 0 < x < \lambda_2 \\ \exp\left[\left(\frac{\lambda_1}{x}\right)^2 - 2\Delta q \ln\left(\frac{\lambda+r_D}{\lambda+x}\right)\right], & \text{for } \lambda_2 < x < \lambda_1 \end{cases} \quad (53)$$

The thickness of the adsorbed layer  $H$  is given by eq 16

$$H \approx \begin{cases} \frac{\lambda_1}{\sqrt{\Delta q}}, & \text{for } \Delta q < \sqrt{fN} \\ R_0 \frac{fN}{\Delta q^{3/2}}, & \text{for } \Delta q > \sqrt{fN} \end{cases} \quad (54)$$

We therefore find that the thickness of the adsorbed layer at large particles is smaller than  $\lambda_1$  because of the charge asymmetry  $\Delta q > 0$ . Thus, charging polyampholytes with the same sign of charge as that of adsorbing particles leads to shaving off the adsorbed layer.

### 3.3. Adsorption Isotherms for Small Particles ( $R < \lambda$ ).

We focus here on *region V* in Figure 2. In this region, the charge of the particle is essentially unscreened,  $Q_{\text{eff}} \approx Q$ , and chains experience the electrostatic potential given by eq 7.

*Henry Regime.* In this regime, the adsorbed molecules do not “feel” their neighbors. At length scales  $0 < x < r_2$ , each polyampholyte molecule forms an “arm” of a star with polarization energy given by eq 38, whereas at length scales  $r_2 < x < r_1$ , polyampholytes adopt stretched “pole” conformations with polarization energy of eq 32. Using the chain polarization energies eqs 38 and 32 together with eq 15, we find the polymer density profile in the dilute adsorbed layer

$$c(x) \approx c_B \begin{cases} \exp\left[Nf^{2/3} \frac{(l_B Q)^{4/3} a^{2/3}}{(x+R)^2}\right], & \text{for } 0 < x < r_2 \\ \exp\left[\left(\frac{r_1}{x}\right)^4\right], & \text{for } r_2 < x < r_1 \end{cases} \quad (55)$$

The polymer surface coverage in the Henry regime is

$$\Gamma_V \approx c_B R \exp\left[Nf^{2/3} \frac{(l_B Q)^{4/3} a^{2/3}}{R^2}\right], \quad \text{for } c_B < c_B^{H*} \quad (56)$$

This regime continues until the polymer concentration at the

particle surface  $c(0)$  reaches the overlap concentration  $c^*$  and adsorbed polyampholytes begin to interact with each other. This upper boundary of the Henry regime is at solution concentration

$$c_B^{H*} \approx c^* \exp\left[Nf^{2/3} \frac{(l_B Q)^{4/3} a^{2/3}}{R^2}\right], \quad \text{region V} \quad (57)$$

Further increase in solution concentration  $c_B > c_B^{H*}$  leads to rearrangement of the adsorbed layer into the semidilute pseudo-star structure.

*Pseudostar Regime.* The polymer density profile in this regime is given by eq 18, where the chain polarization energy  $W_{\text{pol}}^{\text{ch}}(x)$  is determined by eq 38

$$c(x) \approx c^* \sqrt{\ln\left(\frac{c_B}{c^*}\right) + Nf^{2/3} \frac{(l_B Q)^{4/3} a^{2/3}}{(x+R)^2}}, \quad \text{for } 0 < x < H^* \quad (58)$$

The thickness of the inner semidilute part of the adsorbed layer is given by eq 16

$$H^* \approx \frac{N^{1/2} f^{1/3} (l_B Q)^{2/3} a^{1/3}}{\sqrt{\ln(c^*/c_B)}} - R, \quad \text{region V} \quad (59)$$

However, at the length scales  $x > H^*$ , there is still a dilute adsorbed layer with polymer density given by eq 55 and thickness  $r_1$ . The surface coverage

$$\Gamma_V \approx \frac{fN l_B^2 Q^2}{a^2 R^2} \frac{1}{\ln(c^*/c_B)}, \quad \text{for } c_B^{H*} < c_B < c_B^{r_2} \quad (60)$$

is dominated by the semidilute layer and has logarithmic dependence on solution concentration  $c_B$ .

The formation of the adsorbed layer in this range of solution concentrations  $c_B$  can be envisioned as follows. Addition of new molecules to the inner semidilute layer leads to the redistribution of the loops in already adsorbed molecules. The semidilute part of the adsorbed layer with thickness  $H^*$  consists of

$$P(H^*) = N^{-1} (H^*/a)^2 (l_B Q/a)^{2/3} f^{1/3} \quad (61)$$

polyampholyte chains. Equation 61 was obtained by integrating the polymer density profile (eq 58) and by dividing the total number of monomers in the semidilute part of the adsorbed layer by the number of monomers per chain  $N$ . The number of polarized loops with size  $H^*$  per adsorbed molecule  $N/g_{H^*}$  is equal to the degree of polymerization  $N$  divided by the number of monomers  $g_{H^*}$  in the loop of size  $H^*$ . The number of monomers  $g_{H^*}$  in a loop of size  $H^*$  is<sup>17</sup>

$$g_{H^*} \approx (H^*/a)^2 (l_B Q/a)^{-2/3} f^{-1/3} \quad (62)$$

Therefore, the number of large loops per one adsorbed polyampholyte chain

$$N/g_{H^*} \approx N(H^*/a)^{-2} (l_B Q/a)^{2/3} f^{1/3} \quad (63)$$

decreases as the thickness of the inner semidilute adsorbed layer  $H^*$  increases. We note that the number of small loops per chain



(with size  $\approx R$ ) is of the same order of magnitude as the number of large loops:

$$\frac{c(R)R^3}{P(H^*)g_R} \approx N(H^*/a)^{-2}(l_B Q/a)^{2/3} f^{1/3} \quad (64)$$

where  $g_R$  is number of monomers in a small loop that is obtained from eq 62 by substituting  $H^*$  by  $R$ . The thickness of semidilute part of the adsorbed layer  $H^*$  increases with an increase in the solution concentration  $c_B$  leading to a decrease in the total number of polarized loops per adsorbed chain, and the structure of the chain approaches that for a single stretched loop (pole). It follows from eq 63 that for the number of loops per chain  $N/g_{H^*} \approx 1$  the thickness of the semidilute part of the adsorbed layer  $H^*$  reaches the value of  $r_2$  at solution concentration

$$c_B^{r_2} \approx c^* \exp\left(-\frac{r_1^2}{r_2^2}\right), \quad \text{region V} \quad (65)$$

At this concentration  $c_B^{r_2}$  the semidilute part of the adsorbed layer consists of a fully assembled pseudostar.

**Multilayer Regime.** For the interval of solution concentrations,  $c_B^{r_2} < c_B < c^*$ , there are three different parts in the adsorbed layer: pseudo-star at length scales  $0 < x < r_2$  with polymer density given by eq 58; multilayer at  $r_2 < x < H^*$  with polymer density

$$c = c^* \sqrt{\ln\left(\frac{c_B}{c^*}\right) + \left(\frac{r_1}{x}\right)^4}, \quad \text{for } r_2 < x < H^* \quad (66)$$

that is obtained by substituting the polarization energy per chain eq 32 into eq 18; dilute peripheral part of the adsorbed layer at  $H^* < x < r_1$  with polymer density given by eq 55. The peripheral part of the adsorbed layer consists of the stretched poles. The thickness of the semidilute part of adsorbed layer is determined from eq 16

$$H^* \approx \frac{r_1}{\sqrt[4]{\ln(c^*/c_B)}}, \quad \text{for } c_B^{r_2} < c_B < c^* \quad (67)$$

In this range of solution concentrations, the surface coverage depends on the polymer bulk concentration according to eq 19 as follows:

$$\Gamma_V \approx c^* \frac{r_1^3}{R^2 \sqrt[4]{\ln(c^*/c_B)}}, \quad \text{for } c_B^{r_2} < c_B < c^* \quad (68)$$

The saturated adsorbed amount at  $c_B \approx c^*$  is

$$\Gamma_V^{\text{sat}} \approx \frac{r_1^3}{\lambda_3^{1/2} \lambda_1^{1/2} R^2} \quad (69)$$

with saturated value of the layer thickness

$$H^* \approx H_V^{\text{sat}} \approx r_1 \quad (70)$$

**Asymmetric Polyampholytes.** We now consider how the charge asymmetry of a polyampholyte chain,  $\Delta q > 0$ , affects the structure of the adsorbed layer and the adsorption isotherms derived above. The electrostatic energy of repulsion for a chain with net charge  $\Delta q$  located at distance  $x > 0$  from the surface of the particle with charge  $Q$  and radius  $R$  is

$$W_{\text{el}}^{\text{ch}}(x) = kT \frac{\Delta q Q l_B}{x + R} \quad (71)$$

In the Henry regime, the polymer density profile of asymmetric polyampholytes is

$$c(x) \approx c_B \begin{cases} \exp\left[N f^{2/3} \frac{(l_B Q)^{4/3} a^{2/3}}{(x + R)^2} - \frac{\Delta q Q l_B}{x + R}\right], & \text{for } 0 < x < r_2 \\ \exp\left[\left(\frac{r_1}{x}\right)^4 - \frac{\Delta q Q l_B}{x}\right], & \text{for } r_2 < x < r_1 \end{cases} \quad (72)$$

The polymer surface coverage in the Henry regime for asymmetric polyampholytes is

$$\Gamma_V^{\Delta q} \approx c_B R \exp\left[N f^{2/3} \frac{(l_B Q)^{4/3} a^{2/3}}{R^2} - \frac{\Delta q Q l_B}{R}\right], \quad \text{for } c_B < c_B^{H^*} \quad (73)$$

Thus, the polymer surface coverage  $\Gamma$  for asymmetric ( $\Delta q > 0$ ) polyampholytes decreases by the factor  $\exp[\Delta q Q l_B / R]$  in comparison with that for symmetric ( $\Delta q = 0$ ) ones.

In the pole part of the adsorbed layer, the polymer density decays from the particle surface as

$$c(x) \approx c^* \sqrt{\ln\left(\frac{c_B}{c^*}\right) + \left(\frac{r_1}{x}\right)^4 - \frac{\Delta q Q l_B}{x}}, \quad \text{for } r_2 < x < H^* \quad (74)$$

The charge asymmetry not only affects the polymer density distribution but also changes the layer thickness  $H$ . For asymmetric polyampholytes, the adsorption stops at the distance  $H$  from the surface at which the polarization energy of the chain is equal to its direct electrostatic repulsion from the adsorbing small particle:

$$H \approx \begin{cases} l_B^{1/3} \lambda_1^{2/3} Q^{1/3}, & \text{for } \Delta q < \sqrt{fN} \\ \frac{\Delta q^{1/3}}{N^{2/3} l_B^{1/3} a^{2/3} Q^{1/3}}, & \text{for } \Delta q > \sqrt{fN} \end{cases} \quad (75)$$

Thus, for small spherical particles with size  $R$  smaller than the Gouy–Chapman length  $\lambda$  ( $R < \lambda$ ), the thickness of saturated adsorbed layers decreases with increasing charge asymmetry  $\Delta q$  as  $H \sim 1/\Delta q^{1/3}$  for the charge asymmetries  $\Delta q < \sqrt{fN}$  and as  $H \sim 1/\Delta q$  for larger charge asymmetries  $\Delta q > \sqrt{fN}$ .

Following the scheme outlined above, one can derive the adsorption isotherms for all other regions of the adsorption diagram in Figure 2. The results for symmetric polyampholytes with  $\Delta q = 0$  are summarized in the Appendix.

#### 4. Effect of Charge Annealing

The isotherms discussed in the previous section and summarized in the Appendix were derived for the case of polyampholytes with the quenched charges. Example of such polyampholytes are copolymers containing strong acidic and basic groups that are totally dissociated in a wide range of pH. In this case, both the fraction of the charged monomers  $f$  and charge asymmetry  $\Delta q$  have constant values. However, many natural polyampholytes contain weak acidic and basic groups, and the charge on such a molecule depends on the pH (and the ionic strength) of the solution. When such polyampholytes

adsorb on the charged surfaces, the external electric field shifts the ionization equilibrium in the chain making both the fraction of the charged monomers  $f$  and charge asymmetry  $\Delta q$  distance dependent. Adsorption of an “annealed” polyampholyte on a similarly charged surface decreases the net charge asymmetry  $\Delta q$  as the chain approaches the surface (and can even invert the net charge of the molecule), whereas for oppositely charged surface, the charge asymmetry always increases.

To estimate the effect of the “charge annealing” on the features of adsorbed polyampholyte layers, we adopt the following simple model. We assume that each polyampholyte chain contains equal numbers  $N_0$  of acidic and basic groups, and that the degrees of their dissociation  $\alpha_a$  and  $\alpha_b$  are determined by the mass action law:

$$\frac{\alpha_a}{1 - \alpha_a} = \frac{k_a}{\Phi_H} \quad \frac{\alpha_b}{1 - \alpha_b} = \frac{k_b}{\Phi_{OH}} \quad (76)$$

where  $k_a$  and  $k_b$  are the respective dissociation constants of the acidic and basic groups and  $\Phi_H$  and  $\Phi_{OH} = \Phi_0^2/\Phi_H$  are the concentrations of  $H^+$  and  $OH^-$  ions. (Here,  $\Phi_0 = 10^{-7}$  is the concentration of protons in pure water, and the expression for  $\Phi_{OH}$  reflects the association–dissociation equilibrium for water molecules.)

At the isoelectric point (IEP), the concentration of protons is  $\Phi_H = \Phi_{iso}$ ,  $\alpha_a(\Phi_{iso}) = \alpha_b(\Phi_{iso}) = \alpha_{iso}$ , and  $\Delta q = 0$ . Therefore, the dissociation constants in the case of equal number of the acidic and the basic groups are interrelated:

$$\frac{k_a}{k_b} = \left( \frac{\Phi_{iso}}{\Phi_0} \right)^2 \quad (77)$$

Here, the total number of the charged groups

$$M_{iso} = N_0(\alpha_a + \alpha_b) = 2N_0\alpha_{iso} = 2N_0f_0 \quad (78)$$

where  $f_0$  denotes the degree of ionization of the acidic and basic groups at the IEP,  $f_0 = \alpha_{iso} = k_a/(k_a + \Phi_{iso})$ .

When  $\Phi_H < \Phi_{iso}$  or  $\Phi_H > \Phi_{iso}$ , the net charge on the chain increases as

$$\Delta q = N_0 \frac{1 - u^2}{1 + u^2 + u \left( \frac{f_0}{1 - f_0} + \frac{1 - f_0}{f_0} \right)} \quad (79)$$

whereas the total number  $M$  of charged groups changes as

$$M = N_0 \frac{1 + u^2 + 2u \frac{f_0}{1 - f_0}}{1 + u^2 + u \left( \frac{f_0}{1 - f_0} + \frac{1 - f_0}{f_0} \right)} \quad (80)$$

where  $u = \Phi_H/\Phi_{iso}$ . For small deviations from the IEP,  $u = 1 - \delta = 1 - (\Phi_{iso} - \Phi_H)/\Phi_{iso}$ , and for weakly charged chains,  $f_0 \ll 1$ , one finds that the total number of charges  $M \approx 2N_0f_0$  stays almost constant, whereas the charge asymmetry  $\Delta q \approx 2N_0f_0\delta \approx M(\Phi_{iso} - \Phi_H)/\Phi_{iso}$  increases linearly with  $\delta = (\Phi_{iso} - \Phi_H)/\Phi_{iso}$  as  $\Phi_H$  deviates from the IEP.

When such polyampholyte is placed in the external electrostatic potential  $\Delta\Psi(x)$ , the distributions of  $H^+$  and  $OH^-$  ions change as  $\Phi'_H(x) = \Phi_H e^{-\Delta\Psi(x)}$  and  $\Phi'_{OH}(x) = \Phi_{OH} e^{\Delta\Psi(x)}$ , and the degrees of dissociation of ionizable groups depend on the position  $x$  of the chain as

$$\frac{\alpha_a}{1 - \alpha_a} = \frac{k_a}{\Phi_H e^{-\Delta\Psi(x)}} \quad \frac{\alpha_b}{1 - \alpha_b} = \frac{k_b}{\Phi_{OH} e^{\Delta\Psi(x)}} \quad (81)$$

The total number of charges  $M(x)$  changes as

$$M = N_0 \frac{1 + u^2 e^{-2\Delta\Psi(x)} + 2u e^{-\Delta\Psi(x)} \frac{f_0}{1 - f_0}}{1 + u^2 e^{-2\Delta\Psi(x)} + u e^{-\Delta\Psi(x)} \left( \frac{f_0}{1 - f_0} + \frac{1 - f_0}{f_0} \right)} \quad (82)$$

and the net charge  $\Delta q = (\alpha_a - \alpha_b)N_0$  varies with the distance  $x$  from the surface as follows:

$$\Delta q(x) = N_0 \frac{1 - u^2 e^{-2\Delta\Psi(x)}}{1 + u^2 e^{-2\Delta\Psi(x)} + u e^{-\Delta\Psi(x)} \left( \frac{f_0}{1 - f_0} + \frac{1 - f_0}{f_0} \right)} \quad (83)$$

Equation 83 indicates that the position of the IEP,  $x_{iso}$ , in the external potential  $\Delta\Psi(x)$  is given by the following condition:

$$e^{\Delta\Psi(x_{iso})} = u = \frac{\Phi_H}{\Phi_{iso}} \quad (84)$$

For a positively charged planar surface with the electrostatic potential described by eq 3,  $\Delta\Psi(x) = 2 \ln[(\lambda + r_D)/(\lambda + x)] > 0$ , and the isoelectric point exists at  $x < r_D$  only when  $\Phi_H > \Phi_{iso}$ , i.e., only if the polyampholyte in the bulk solution is positively charged. For a negatively charged surface,  $\Delta\Psi(x) = -2 \ln[(\lambda + r_D)/(\lambda + x)] < 0$ , and the isoelectric point exists at  $x < r_D$  only if the polyampholyte chain is negatively charged in the bulk solution,  $\Phi_H < \Phi_{iso}$ . We note that at distances  $x < x_{iso}$  the net charge on the annealed polyampholyte  $\Delta q$  reverses its sign.

## 5. Discussion

We describe a scaling model of the adsorption of polyampholytes at charged spherical particles. The isotherms for polyampholyte adsorption at charged particles were calculated as functions of radius and charge on the particles and of the fraction of ionized groups of polyampholyte molecules. Our analysis shows that the surface coverage changes noticeable only at extremely low and marginal solution concentrations  $c_B$ . In the Henry regime, the surface coverage  $\Gamma$  grows linearly with solution concentration  $c_B$ , whereas in all other regimes,  $\Gamma$  increases with  $c_B$  as  $[\ln(c_B/c^*)]^\alpha$  ( $\alpha = -1$  or  $-1/4$ , see the Appendix) or demonstrates even weaker,  $\ln(\ln(c_B/c^*))$ , dependence as indicated by eq 49. Therefore, to compare our theoretical predictions with experimental observations, we have to focus on the experimental data in the Henry and the saturated (plateau) regimes of the adsorption isotherms measured at  $c_B \leq c^*$ .

There are three parts of the adsorption isotherm:

(i) **Henry regime**, in which the adsorbed layer is dilute and the energy gain by adsorbed chains in this layer is balanced by the entropy lost due to localization of these chains from exponentially dilute solution with concentration  $c_B < c_B^{H*}$ . The thickness of the adsorbed layer is  $\lambda_1$  for large particles and  $r_1$  for small ones.

(ii) **Pseudobrush regime (pseudostar regime** for small particles). In this regime of the adsorption isotherm, the semidilute part of the adsorbed layer of thickness  $H^*$  exists and dominates most of the layer properties. Chains in this part of the adsorbed layer form an unsaturated pseudobrush for large

particles and an unsaturated pseudostar for small ones. The thickness of this pseudobrush (pseudostar) increases logarithmically with solution concentration  $c_B$ .

(iii) **Multilayer regime.** Semidilute part of the adsorbed layer of thickness  $H^*$  consists of a saturated pseudobrush of thickness  $\lambda_2$  (a pseudostar of thickness  $r_2$ ) and a semidilute part of multilayer of stretched chains at distances  $\lambda_2 < x < H^*$  ( $r_2 < x < H^*$ ) from the particle surface. There is still a dilute part of adsorbed layer for  $H^* < x < \lambda_1$  ( $H^* < x < r_1$ ) from the particle surface consisting of dilute stretched chains strongly attracted to the particle.

To check the predictions of our model we consider experimental data on adsorption of gelatin at charged spherical particles. The adsorption of gelatin on polystyrene latex and silica particles at various pH and ionic strengths of the solution was investigated recently in ref 29. The hydrodynamic diameter  $D_h$  of the particles was determined as a function of gelatin solution concentration  $c_B$  from the measurements of the apparent diffusion constant of particles with adsorbed gelatin layer and the viscosity of the latex/gelatin solution. The thickness of the adsorbed gelatin layer  $H^*$  was estimated by subtracting the hydrodynamic diameter of a bare particle  $D_h^0 = 135$  nm from the diameter  $D_h$  of the particle covered with gelatin,  $H^* \approx (D_h - D_h^0)/2$ . To check the predictions of our model, we consider the experimental data for the salt-free solutions and for the value of pH = 5.5. This value of pH is higher than the value of pH = 4.9, corresponding to the isoelectric point of gelatin, indicating that gelatin molecules are negatively charged. The polystyrene particles are also negatively charged with the surface charge density  $\sigma = 1/82 \text{ \AA}^{-2}$  elementary charges per unit area. (This surface charge corresponds to the value of the Gouy–Chapman length  $\lambda \approx 2 \text{ \AA}$ ). The behavior of gelatin in aqueous solutions indicates that it is an annealed polyampholyte with pH-dependent charge on the chains. Adsorption of such polymers is accompanied by the adjustment of the charge, and therefore, ionization of the adsorbed molecules (and net charge  $\Delta q$ ) will vary with distance  $x$  from the adsorbing particle. According to our model, such chains should reduce their net charge in the adsorbed layer at distance  $x < r_D$ . For the bulk solution with pH = 5.5 and no added salt, the Debye radius is governed by the concentration of protons and is estimated to be  $r_D \approx 43$  nm. According to eq 84, the isoelectric point is located within the adsorbed layer at

$$x_{\text{iso}} = (\lambda + r_D) \left( \frac{\Phi_H}{\Phi_{\text{iso}}} \right)^2 - \lambda \approx 20 \text{ nm} \quad (85)$$

To check the predictions of our model, we use the data from ref 29 in the range of gelatin solution concentrations below the overlap threshold  $c^*$  that is estimated to be at 6–7 mg/mL.

Figure 7 shows the experimental dependence of  $H^{*-2}$  (measured in  $\text{nm}^{-2}$ ) as a function of  $\ln(c_B)$  in the range of solution concentrations  $c_B < c^*$ . According to the results of our scaling model (eq 54), one expects in these coordinates a straight line with the slope of the order of  $\lambda_1^{-2} \approx (a^2 f N^2)^{-1}$ . We find that not too close to the overlap concentration  $c^*$ , the experimental data fits reasonably well by line with the slope equal to  $6.25 \times 10^{-4} \text{ nm}^{-2}$  (shown by the solid line). As solution concentration  $c_B$  approaches the overlap concentration  $c^*$ , the experimental points deviate from the theoretical curve. This is not surprising because our model uses the expression for the chemical potential of polyampholyte molecules in dilute solutions. At concentrations close to the overlap concentration  $c_B \approx c^*$ , the nonelectrostatic interactions in the solution essentially

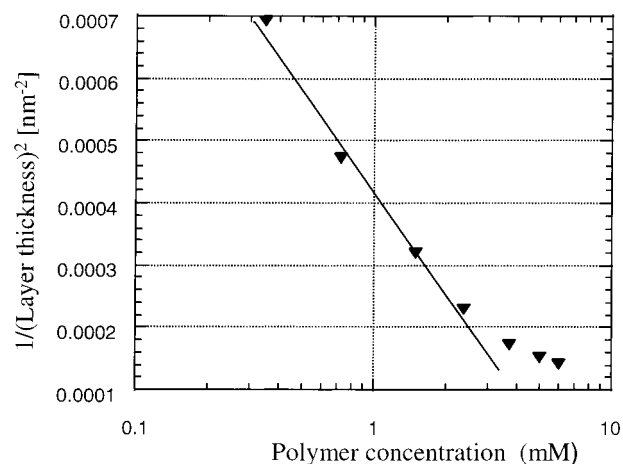


**Figure 7.** Adsorption isotherm for gelatin at latex particles at solution pH = 5.5 (experimental data from ref 29). Solid line: theoretical prediction eq 54.

modify the bulk chemical potential  $\mu_B$ , and deviations from the predicted  $H^*$  versus  $c_B$  dependence are expected.

The value of the slope gives us an estimate for the parameter  $\lambda_1 \approx a f^{1/2} N \approx 40$  nm. Assuming that gelatin is a typical flexible polymer with number of monomers  $N \approx 10^3$  and the average size of a monomer  $a = 3 \text{ \AA} = 0.3$  nm, we estimate  $f \approx 0.019$ . This value is at the boundary of solubility of polyampholyte chain with this degree of polymerization given by eq 2. It follows from this estimate that the total number of dissociated groups  $M \approx fN$  on the polyampholyte molecule is surprisingly low,  $fN \approx 19$ , and that the average number of monomers between the charges is  $1/f \approx 56$ . We note, however, that a gelatin molecule has on average  $m \approx 6$  neutral monomers between the ionizable groups. Therefore, in the framework of our model, the degree of ionization of acidic and basic groups at the isoelectric point is estimated to be  $f_0 = fm \approx 0.1$ .

We now analyze the Henry regime of the adsorption isotherms investigated for a similar system in ref 30. Here, the adsorption of gelatin on latex particles was monitored by a fluorescence technique. The polystyrene particles had hydrodynamic radius  $R_h^0 = 37$  nm and the surface charge density  $\sigma = 1/148 \text{ \AA}^{-2}$ . This surface charge density corresponds to the value of the Gouy–Chapman length  $\lambda \approx 3 \text{ \AA}$ . For such a small value of the Gouy–Chapman length  $\lambda$ , the adsorbed polyampholyte molecules in the Henry regime are expected to adopt the “pancake” conformation with the thickness of  $H_{\text{char}} \approx \lambda_3 = a f^{-1/2}$ . For  $a = 3 \text{ \AA}$  and  $f \approx 1.9 \times 10^{-2}$  (as estimated earlier from the plateau values of the adsorption isotherms), we find  $H \approx 22 \text{ \AA}$ . The experiments were performed at the ionic strength of the gelatin/latex system  $I = 0.01$  N that corresponds to the value of the Debye radius  $r_D \approx 36 \text{ \AA}$ . In this range of salt concentrations,  $r_D > H_{\text{char}}$ , and therefore, one can apply the results of our salt-free model to analyze the adsorption isotherms in ref 30.

The data in ref 30 clearly indicates that the initial slope of the adsorption isotherms in the gelatin/polystyrene latex system is almost independent of the temperature (in the studied range 20–40 °C) and the value of the partition coefficient, that relates the average concentration of polymer in the adsorbed layer to the gelatin concentration, is close to 10. In the framework of our model, the partition coefficient  $K$  for asymmetric polyampholyte in the Henry regime can be estimated as

$$K = \exp(Nf - \Delta q) \quad (86)$$

We note that eqs 83 and 82 give estimates for the charge

asymmetry  $\Delta q(x)$  and for the total number of the charged groups  $Nf(x)$  when the chain size  $L(x) \ll x$ . Applying eqs 83 and 82 to estimate the charge asymmetry  $\Delta q$  on the adsorbed chain and using the following values of the parameters— $2N_0 \approx 160$  (total number of ionizable groups in gelatin molecule),  $f_0 \approx 0.1$  (as estimated from the thickness of saturated adsorbed layers),  $\lambda = 3 \text{ \AA}$ ,  $r_D = 36 \text{ \AA}$ , and  $H_{\text{char}} \approx 22A$ —we find  $fN \approx 22$  and  $\Delta q \approx 19$ . This theoretical estimate for the partition coefficient  $K = \exp(22-19) \approx \exp(3)$  is indeed close to the experimental value  $K = 10$ .

Thus, our theory of polyampholyte adsorption at charged particles gives a qualitatively reasonable interpretation of the experimental results using only the electrostatic nature of polyampholyte adsorption without invoking any additional assumptions about specific interactions of polyampholytes with adsorbing surface. Of course, our theory does not cover all aspects of polyampholyte adsorption. We leave aside the questions of (i) the effect of specific interactions (hydrophobic interactions and formation of hydrogen bonds) between a polymer backbone and an adsorbing surface and (ii) the effect of the difference in the dielectric constants of solvent and adsorbing substrate on polyampholyte adsorption. The detailed analysis of these effects requires special considerations and will be addressed in a separate publication. However, it is possible to comment on the qualitative effect of the specific interactions between adsorbed polyampholytes and the surface. These

interactions are short-ranged and will only influence the conformations of the chains and, as a consequence, the structure of the adsorbed layer in the immediate vicinity to the adsorbing surface, leaving the multilayers structure of the adsorbed polyampholytes unchanged. The structure of adsorbed multilayers beyond the range of the specific interactions is preserved by the long-ranged nature of polarization-induced attraction between the charged surface and polyampholytes. The difference in the dielectric constants of the adsorbing substrate and the solvent can only lead to some quantitative corrections and will not change the qualitative picture of polyampholyte adsorption described in the present paper.

**Acknowledgment.** The financial support of the NSF under Grants DMR-9730777 and DMR-0102267 and of the Eastman Kodak Company is gratefully acknowledged. The authors are grateful to Dr. T. Whitesides for valuable discussions.

## Appendix

We summarize here the polymer surface coverage  $\Gamma$ , thickness  $H_{\text{char}}$  for solution concentrations  $c_B < c_B^{H^*}$ , and the thickness  $H^*$  of the semidilute part of the adsorbed layer for  $c_B^{H^*} < c_B < c^*$  in various regions of the adsorption diagram in Figure 2. The scaling expressions employ the Gouy–Chapman length  $\lambda \approx 1/b\sigma$ ; lengths  $\lambda_1 \approx af^{1/2}N$ ,  $\lambda_2 \approx af^{1/4}N^{3/4}$ , and  $\lambda_3 \approx$

### Region I ( $R > \lambda_1$ , $\lambda_2 < \lambda < \lambda_1$ )

$\frac{c_B}{c^*} < \frac{\lambda_1}{\lambda} \exp\left[-\frac{\lambda_1^2}{\lambda^2}\right]$	$\Gamma \simeq c_B \lambda \exp\left[\frac{\lambda_1^2}{\lambda^2}\right]$	$H_{\text{char}} \simeq \lambda$
$1 > \frac{c_B}{c^*} > \frac{\lambda_1}{\lambda} \exp\left[-\frac{\lambda_1^2}{\lambda^2}\right]$	$\Gamma \simeq a^{-2} \left(\frac{\lambda_1}{\lambda_2}\right)^2 \ln \frac{\lambda_1}{\lambda \left[\ln\left(\frac{c^*}{c_B}\right)\right]^{1/2}}$	$H^* \simeq \frac{\lambda_1}{\left[\ln\left(\frac{c^*}{c_B}\right)\right]^{1/2}}$

### Region II ( $R > \lambda_1$ , $\lambda_3 < \lambda < \lambda_2$ )

$\frac{c_B}{c^*} < \frac{\lambda_2^{2/3}}{\lambda_3^{1/3} \lambda^{1/3}} \exp\left[-\frac{\lambda_2^{4/3}}{\lambda_3^{2/3} \lambda^{2/3}}\right]$	$\Gamma \simeq c_B \lambda \exp\left[\frac{\lambda_2^{4/3}}{\lambda_3^{2/3} \lambda^{2/3}}\right]$	$H_{\text{char}} \simeq \lambda$
$\frac{\lambda_2^{2/3}}{\lambda_3^{1/3} \lambda^{1/3}} \exp\left[-\frac{\lambda_2^{4/3}}{\lambda_3^{2/3} \lambda^{2/3}}\right] < \frac{c_B}{c^*} < \exp\left[-\frac{\lambda_2^2}{\lambda_1 \lambda_3}\right]$	$\Gamma \simeq a^{-2} \frac{\lambda_1}{\lambda_3} \frac{1}{\ln\left(\frac{c^*}{c_B}\right)}$	$H^* \simeq \frac{\lambda_2^2}{\lambda_3} \frac{\lambda_1}{\left[\ln\left(\frac{c^*}{c_B}\right)\right]^{3/2}}$
$\exp\left[-\frac{\lambda_2^2}{\lambda_1 \lambda_3}\right] < \frac{c_B}{c^*} < 1$	$\Gamma \simeq a^{-2} \left(\frac{\lambda_1}{\lambda_2}\right)^2 \ln \frac{\lambda_1}{\lambda_2 \left[\ln\left(\frac{c^*}{c_B}\right)\right]^{1/2}}$	$H^* \simeq \frac{\lambda_1}{\left[\ln\left(\frac{c^*}{c_B}\right)\right]^{1/2}}$

### Region III ( $R > \lambda_1$ , $\lambda_3 < \lambda$ )

$\frac{c_B}{c^*} < \frac{\lambda_2^{2/3}}{\lambda_3^{1/3} \lambda^{1/3}} \exp\left[-\frac{\lambda_2^{4/3}}{\lambda_3^{2/3} \lambda^{2/3}}\right]$	$\Gamma \simeq c_B \lambda_3 \exp\left[\frac{\lambda_2^{4/3}}{\lambda_3^{2/3} \lambda^{2/3}}\right]$	$H_{\text{char}} \simeq \lambda_3$
$\frac{\lambda_2^{2/3}}{\lambda_3^{1/3} \lambda^{1/3}} \exp\left[-\frac{\lambda_2^{4/3}}{\lambda_3^{2/3} \lambda^{2/3}}\right] < \frac{c_B}{c^*} < \exp\left[-\frac{\lambda_2^2}{\lambda_1 \lambda_3}\right]$	$\Gamma \simeq a^{-2} \frac{\lambda_1}{\lambda_3} \frac{1}{\ln\left(\frac{c^*}{c_B}\right)}$	$H^* \simeq \frac{\lambda_2^2}{\lambda_3} \frac{\lambda_1}{\left[\ln\left(\frac{c^*}{c_B}\right)\right]^{3/2}}$
$\exp\left[-\frac{\lambda_2^2}{\lambda_1 \lambda_3}\right] < \frac{c_B}{c^*} < 1$	$\Gamma \simeq a^{-2} \left(\frac{\lambda_1}{\lambda_2}\right)^2 \ln \frac{\lambda_1}{\lambda_2 \left[\ln\left(\frac{c^*}{c_B}\right)\right]^{1/2}}$	$H^* \simeq \frac{\lambda_1}{\left[\ln\left(\frac{c^*}{c_B}\right)\right]^{1/2}}$

### Region Ia ( $\lambda_2 < \lambda < \lambda_1$ , $R > \lambda$ )

$\frac{c_B}{c^*} < \frac{\lambda_1}{\lambda_2} \exp\left[-\frac{\lambda_1^2}{\lambda_2^2}\right]$	$\Gamma \simeq c_B \lambda \exp\left[\frac{\lambda_1^2}{\lambda_2^2}\right]$	$H_{\text{char}} \simeq \lambda$
$\frac{\lambda_1}{\lambda_2} \exp\left[-\frac{\lambda_1^2}{\lambda_2^2}\right] < \frac{c_B}{c^*} < \frac{\lambda_1}{R} \exp\left[-\frac{\lambda_1^2}{R^2}\right]$	$\Gamma \simeq a^{-2} \left(\frac{\lambda_1}{\lambda_2}\right)^2 \ln \frac{\lambda_1}{\lambda \left[\ln\left(\frac{c^*}{c_B}\right)\right]^{1/2}}$	$H^* \simeq \frac{\lambda_1}{\left[\ln\left(\frac{c^*}{c_B}\right)\right]^{1/2}}$
$\frac{\lambda_1}{R} \exp\left[-\frac{\lambda_1^2}{R^2}\right] < \frac{c_B}{c^*} < 1$	$\Gamma \simeq a^{-2} \frac{\lambda_1^{5/2}}{\lambda_2^2 R^{1/2}} \frac{1}{\left[\ln\left(\frac{c^*}{c_B}\right)\right]^{1/4}}$	$H^* \simeq \frac{\lambda_2}{\left[\ln\left(\frac{c^*}{c_B}\right)\right]^{1/4}}$





$af^{-1/2}$ ; and the radius of the particle  $R$ . The boundaries for each regime are indicated in the brackets.

## References and Notes

- (1) Tanford, C. *Physical Chemistry of Macromolecules*; Wiley: New York, 1961.
- (2) de Gennes, P.-G.; Badoz, J. *Fragile Objects*; Springer-Verlag: New York, 1996.
- (3) Ward, A. G.; Courts, A. *The Science and Technology of Gelatin*; Academic Press: New York, 1977.
- (4) Cox, R. J. *Photographic Gelatin*; Academic Press: New York, 1972.
- (5) Curme, H. G.; Natale, C. C. *J. Phys. Chem.* **1964**, *68*, 3009.
- (6) Berendsen, R.; Borginon, H. *J. Photogr. Sci.* **1968**, *16*, 194.
- (7) Maternaghan, T.; Banghan, O. B.; Ottewill, R. H. *J. Photogr. Sci.* **1980**, *28*, 1.
- (8) Kudish, A. T.; Eirich, F. R. *Proteins at Interfaces*; American Chemical Society: Washington, D.C., 1987; Vol. 261.
- (9) Kawanishi, N.; Christenson, H.; Ninham, B. *J. Phys. Chem.* **1990**, *94*, 4611.
- (10) Vaynberg, A. K.; Wagner, N. J.; Sharma, R.; Martic, P. *J. Coll. Interface Sci.* **1998**, *205*, 131.
- (11) Kamiyama, Y.; Israelachvili, J. *Macromolecules* **1992**, *25*, 5081.
- (12) Neyret, S.; Ouali, L.; Candau, F.; Pefferkorn, E. *J. Coll. Interface Sci.* **1995**, *187*, 86.
- (13) Fleer, G. J.; Cohen Stuart, M. A.; Scheutjens, J. M. H. M.; Gasgove, T.; Vincent, B. *Polymer at Interfaces*; Chapman and Hall: London, 1993.
- (14) Dobrynin, A. V.; Rubinstein, M.; Joanny, J.-F. *Macromolecules* **1997**, *30*, 4332.
- (15) Netz, R.; Joanny, J.-F. *Macromolecules* **1998**, *31*, 5123.
- (16) Dobrynin, A. V.; Obukhov, S., P.; Rubinstein, M. *Macromolecules* **1999**, *32*, 5689.
- (17) Dobrynin, A. V.; Zhulina, E. B.; Rubinstein, M. *Macromolecules* **2001**, *34*, 627.
- (18) Zhulina, E. B.; Dobrynin, A. V.; Rubinstein, M. *Eur. Phys. J. E* **2001**.
- (19) Daoud, M.; Cotton, J.-P. *J. Phys. (Paris)* **1982**, *43*, 531.
- (20) Birshtein, T. M.; Zhulina, E. B. *Polymer* **1984**, *25*, 1453.
- (21) Higgs, P. G.; Joanny, J. F. *J. Chem. Phys.* **1988**, *89*, 5273.
- (22) Kantor, Y.; Kardar, M.; Li, H. *Phys. Rev. Lett.* **1992**, *69*, 61; *Phys. Rev. E* **1994**, *49*, 1383.
- (23) Kantor, Y.; Kardar, M. *Europhys. Lett.* **1994**, *27*, 643; *Phys. Rev. E* **1995**, *51*, 1299; **1995**, *52*, 835.
- (24) Dobrynin, A. V.; Rubinstein, M. *J. Phys. II (France)* **1995**, *5*, 677.
- (25) Everaers, R.; Johner, A.; Joanny, J.-F. *Europhys. Lett.* **1997**, *37*, 275.
- (26) Israelachvili, J. N., *Intermolecular and Surface Forces*; Academic Press: London, 1991.
- (27) Safran, S. A. *Statistical Thermodynamics of Surfaces, Interfaces, and Membranes*; Addison-Wesley: Reading, MA, 1994.
- (28) It is important to point out that the polymer concentration  $c(x) \approx c^*$  corresponds to energetic (the energy of ternary contacts per chain is of the order of the thermal energy  $kT$ ) rather than geometric overlap of polyampholyte chains. The two overlaps are different because of chain stretching.
- (29) Hone, J. H. E.; Howe, A. M.; Whitesides, T. H. *Colloids Surf. A* **2000**, *161*, 283.
- (30) Vaynberg, K. A.; Wagner, N. J.; Sharme, R.; Martic, P. *J. Colloid Interface Sci.* **1998**, *205*, 131.